Catal Lett (2015) 145:162–172
DOI 10.1007/s10562-014-1438-7

Factors Controlling the Acidity of Zeolites

Mercedes Boronat · Avelino Corma

Received: 3 November 2014 / Accepted: 12 November 2014 / Published online: 19 December 2014

Abstract Most industrial applications of zeolites as catalysts rely on their Brönsted acidity properties. However, neither quantifying acid strength in solids nor correlating acidity with catalytic activity is straightforward. The ease and speed at which the proton transfer process occurs in zeolites depends on different factors, including the concentration of active sites and local geometry around them, the ability of base molecules to diffuse through channels and cavities close to the acid sites, and the stabilization of ionic transition states and intermediates by electrostatic interactions with the zeolite framework. All these aspects are analyzed in this review based on experimental characterization data (FTIR spectroscopy of hydroxyl groups and adsorbed probe molecules, in situ MAS-NMR of reactants and intermediates, TPD and microcalorimetry of adsorbed probe molecules) and computational studies.

Keywords Catalysis · Zeolites · Brönsted acidity · Reactivity

1 Introduction

Zeolites have been used as solid acid catalysts for hydrocarbon reactions since the early 60 s, largely due to their high catalytic activity and thermal stability. They have found wide applications in oil refining, petrochemistry and fine chemical production industries for Brönsted acid catalyzed reactions such as cracking, hydrocracking, isomerization and alkylation of hydrocarbons, as well as methanol to olefins (MTO), methanol dehydration or carbonylation processes [1–8]. Due to the large scale application of acid zeolites, considerable research efforts have been devoted to characterize and quantify the number and strength of the zeolite acid sites, with the aim of optimizing the catalyst design [9–14]. Zeolites are crystalline aluminosilicates whose framework is composed by SiO_4 and AlO_4 tetrahedra linked through shared corner O atoms, forming a three-dimensional microporous structure of channels and cavities of molecular dimensions. The presence of trivalent Al^{3+} species in the framework generates a net negative charge that is compensated by cations like Na^+, K^+ Mg^{2+}, Ca^{2+}, NH_4^+, or protons H^+. In this last case, zeolites with strong Brönsted acidity can be generated. Moreover, the microporous structure of zeolites provides a large internal surface area that allows a large concentration of active sites accessible to reactants, together with notable selectivity effects related both to diffusion of reactants and products inside the pore system and to steric constraints on intermediates and transition states. All these features influence the overall catalytic performance of acid zeolites, and make difficult to establish an acidity scale and a clear correlation between acidity and catalytic activity. It has also to be considered that, contrary to what occurs with acid molecules in gas or liquid phases, solid catalysts are heterogeneous in nature and contain a distribution of sites with different intrinsic acid strength associated to differences in local structure, chemical environment or location within the channels. All these aspects of zeolites acidity have been previously analyzed by different authors [9–14], and an overview of the most important aspects is now presented and discussed in this contribution.

M. Boronat · A. Corma (✉)
Instituto de Tecnología Química, Universidad Politécnica de Valencia – Consejo Superior de Investigaciones Científicas, Av. los Naranjos, s/n, 46022 Valencia, Spain
e-mail: acorma@itq.upv.es

2 Intrinsic Acidity of Brönsted Sites in Zeolites

The Brönsted acid sites correspond to bridged hydroxyl groups, Si–O(H)–Al, formed by a proton directly bonded to a framework oxygen atom connecting one Al and one Si atom (Fig. 1). The bridged hydroxyl group was initially described as a silanol group, SiOH, activated by the presence of a neighboring Al^{3+} Lewis acid center, but it was later considered that all three O–Al, O–Si and O–H bonds are strong covalent bonds superposed by small electrostatic interactions [9, 11, 15]. The O atom in this non-classical bonding situation has a formal threefold coordination similar to that present in the hydronium cation H_3O^+, where the three H–O–H angles tend to be similar and take values around 120°. The preferred geometry for the Al–O(H)–Si group would involve a narrowing of the Al–O–Si angle with respect to the deprotonated system, but this is prevented or minimized by the long-range ordering of the zeolite crystal. The strong acidity of bridged hydroxyl groups can therefore attributed to the threefold coordination of the O atom and the geometry restrictions imposed by the crystalline structure.

3 Quantifying Acidity by Deprotonation Energies. The Relevance of the Zeolite Models Used

According to Brönsted definition [16], an acid is a species with a tendency to donate a proton:

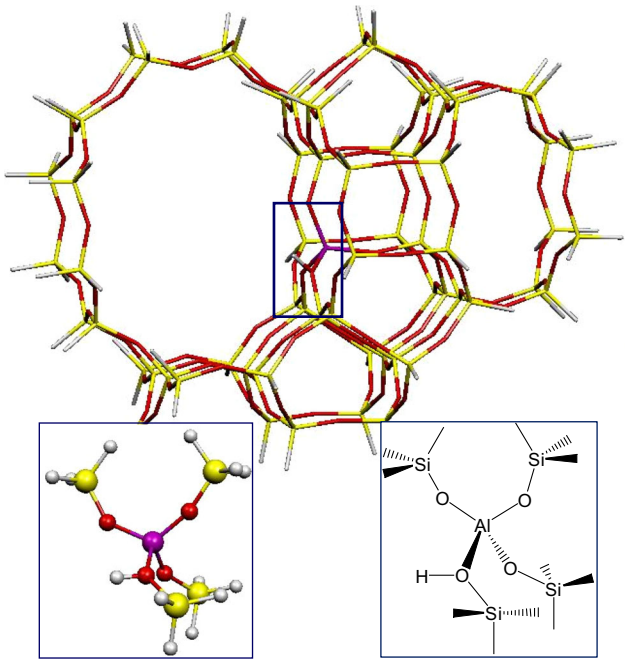

Fig. 1 Structure of Brönsted acid sites in zeolites

$$AH \rightarrow A^- + H^+.$$

In a first approximation the intrinsic acidity of a Brönsted acid site could be characterized by the deprotonation energy (DPE), defined as the energy necessary to separate a proton to infinite distance from the resulting anion:

$$DPE = E(A^-) + E(H^+) - E(AH).$$

While this magnitude cannot be properly measured by experiment, it can be estimated from quantum-chemical calculations. Early theoretical studies of isomorphously substituted MFI zeolites found that calculated deprotonation energies, also named proton affinities (PA) in some cases, correctly reproduced the experimental trend in acid strength: B–OH–Si < Fe–OH–Si < Ga–OH–Si < Al–OH–Si [17–19]. In the case of aluminosilicates, extensive investigation of deprotonation energies of H-ZSM-5 zeolite by Brand et al. evidenced that calculated DPE values depend on the type and size of the zeolite model used [20, 21]. When a cluster model is used to represent the Brönsted acid site, the calculated DPE values slowly converge with cluster size, with variations as large as 30 kcal/mol with each additional shell. Relaxation of the geometry around the bridged hydroxyl group can increase the DPE values by 15–55 kcal/mol, this effect being mainly related to the broadening of the Si–O–Al angle upon deprotonation. Indeed, the local geometry of the Al–O(H)–Si group seems to be an important parameter influencing acidity. Thus, the range of T–O–T angles in strongly acidic zeolites like H-SZM-5 (137°–177°) or mordenite (143°–180°) is larger than on less acidic materials like HY (138°–147°). Theoretical studies using small cluster models found that deprotonation energies increase with increasing the Si–O–Al angle, and that the most stable angles for protonated and deprotonated forms of the bridging hydroxyl group are 134° and 179°, respectively [9, 15, 22]. For clusters containing more than 20 T-atoms deprotonation energies converge, suggesting that electrostatic interactions in models of this size already approach those present in real zeolites. A very recent DFT study of the electron density differences between neutral and deprotonated MFI structures has shown that long range electrostatic effects play a lesser role and, instead, polarization of the Si–O bonds and atoms up to the second O-atom coordination sphere is essential to stabilize the negative charge generated by deprotonation [23]. The order of acidity of isomorphously substituted MFI zeolites is correctly reproduced no matter the size of the model employed [17–19, 24], but to accurately characterize the acid strength of Al-containing zeolites high level calculations and large models are required. Thus, when cluster models treated with quantum chemical methods are embedded in a periodic system described by interatomic potentials, that is, the QM-Pot approach, the

influence of cluster size is small, and all calculated DPE values stay within a narrow range of 1250–1253 kJ/mol for FAU and of 1281–1287 kJ/mol for MFI structures. The embedded cluster QM-Pot approach permits to establish an acidity scale for Brönsted acid sites in zeolites with different framework structure, that agrees with results obtained using more demanding periodic DFT calculations. According to theory, acidity order is: H-SAPO-34 < H-ZSM-5 < H-MOR < H-SSZ-13 < H-FAU < H-silicalite [25, 26].

Haase and Sauer performed ab initio molecular dynamics simulations on various zeolites with different framework structure (CHA, TON, FER and MFI) and found that all calculated deprotonation energies were within 21 kJ/mol. However, when these DPE values were compared with methanol adsorption energies, taken as another way of measuring acidity, no systematic correlation was found [27]. And a similar mismatching was obtained when comparing DPE with ammonia adsorption energies, evidencing the difficulties to consistently quantify zeolite acidity [28, 29].

4 The Strength of the OH Bond as a Measure of Acidity

It can also be considered that the intrinsic acidity of a Brönsted acid site is inversely proportional to the strength of the O–H bond. In this line, spectroscopic properties like the vibrational frequency of the hydroxyl group ν(OH) in IR spectra and the ^{1}H NMR chemical shift of the proton in the Si–O(H)–Al group have been widely used to measure the strength of the O–H bond [10, 30, 31]. Zeolites typically contain two types of hydroxyl groups, bridged hydroxyl groups Si–O(H)–Al responsible for Brönsted acidity and silanol groups SiOH associated to crystal termination or defects in the framework. In some cases, hydroxyl groups associated to extra-framework Al species Al–OH are also present. The stretching vibrational frequency ν(OH) is related to the acid strength: the lower the stretching frequency, the weaker the OH bond and therefore the higher the acid strength. Thus, while the typical IR bands associated to silanol groups in zeolites appear around 3750 cm^{-1}, the acidic bridged hydroxyl groups are observed in the region between 3550 and 3650 cm^{-1} [30, 32]. However, this view is too simple, and other factors like the presence of close Al centers, defects in the crystalline structure, or the location of the Brönsted sites within channels of different dimensions can modify the ν(OH) frequency. The IR spectra of H-ZSM-5 zeolite shows, besides the acidic hydroxyl appearing at 3605 cm^{-1} and external silanol groups at 3740 cm^{-1}, a third broad feature centered at ~3500 cm^{-1} associated to nested silanols at a cation vacancy defect [33]. In the IR spectra of H-Y zeolite two features corresponding to bridged hydroxyl groups are observed: a high frequency (HF) band at 3650 cm^{-1} assigned to hydroxyl groups pointing to the supercage of the FAU structure, and a low frequency (LF) signal at 3540 cm^{-1} assigned to bridged hydroxyl groups located in the six-membered rings of the sodalite cage. Interestingly, only the HF feature corresponding to a stronger OH bond leads to characteristic Brönsted acid activity [34].

A similar reasoning can be applied to ^{1}H NMR spectroscopy. A weaker OH bond (or a stronger acid center) should be associated to a larger net atomic charge on the proton, that is, a lower shielding σ_H and therefore a larger shift δ_H in the NMR spectra. Moreover, NMR spectroscopy is a quantitative characterization tool, since the intensity of NMR peaks is proportional to the number of atoms present. Five signals can be observed in the ^{1}H NMR spectra of HY zeolites: a signal at 1.8–2.3 ppm due to silanol SiOH groups at the crystal surface, a signal between 2.5 and 3.6 ppm due to extraframework Al–OH species, a peak 6.5–7.0 ppm corresponding to residual NH_4^+ cations, and two different signals attributed to bridged hydroxyl groups. One of them at 3.8–4.4 ppm is assigned to Si–O(H)–Al groups with the proton pointing toward the zeolite supercage and is related to the HF IR band at 3650 cm^{-1}, and the other one at 5 ppm is assigned to the bridged hydroxyl groups in the sodalite cage and related to the LF IR band at 3540 cm^{-1} [31].

Combination of FTIR and ^{1}H NMR spectroscopies provides a detailed characterization of acid sites in zeolites, and has allowed for instance to follow the evolution of the different hydroxyl groups in chabazite during activation at increasing temperature [35]. The as-synthesized samples show the typical features corresponding to silanol groups and residual NH_4^+, very low amounts of extra-framework Al–OH species, and two types of Brönsted acid sites: HF bridged hydroxyls in the eight-member ring channels of CHA structure, and LF bridged hydroxyls in the six-member ring of the sodalite cages. Activation of these samples at 450–550 °C leads to ammonia desorption and formation of extra-framework Al–OH species by framework dealumination, that occurs primarily at the LF Brönsted site. Raising activation temperature to 650 °C leads to disappearing of the LF and HF Brönsted sites together with a growth of the Al–OH and SiOH signals, which is consistent with formation of framework defects due to extensive dealumination.

The presence of more than one component in the IR band associated to Brönsted acid sites in zeolites has also been described for H-FER [36, 37] and H-MOR [38, 39]. The bi-dimesional channel system of FER is composed by ten-membered ring (10-MR) channels parallel to the *c* axis interconnected by eight-membered ring (8-MR) channels parallel to *b*. The MOR framework is composed by four-

and five-membered rings which link to form large 12-MR channels parallel to *c* interconnected via 8-MR side pockets parallel to *b* (Figure 2). Analysis of the changes in the OH region of the IR spectra of H-FER and H-MOR observed during adsorption of probe molecules of varying size allowed to determine the location and accessibility of the different types of Brönsted acid sites observed. Thus, it was possible to identify hydroxyl groups within 10-MR ($\sim$3600 cm^{-1}) and 8-MR ($\sim$3590 cm^{-1}) channels in H-FER, and hydroxyl groups within 12-MR channels ($\sim$3610 cm^{-1}) and in 8-MR side pockets ($\sim$3590 cm^{-1}) in H-MOR. Singular value decomposition (SVD) analysis of the OH region of the IR spectra at different concentration of adsorbed probe molecules allowed even to quantify the fraction of the OH groups within channels of different size. A third ν(OH) component at 3605 cm^{-1} in the IR band of H-MOR was observed and was ascribed to Brönsted centers located at the intersection between the 12-MR channels and the 8-MR side pockets [38, 40]. It is important to remark that, in these cases, the differences in vibrational frequencies are not related to differences in acid strength but to the dimensions of the channels where the Brönsted sites are located, and to a stronger interaction of the acidic protons with neighboring O atoms in the smaller channels or pockets [41].

While it is clear that analysis of IR spectra in the ν(OH) vibration frequency region, sometimes in combination with ^{1}H NMR spectroscopy, provides accurate information about the nature, location and accessibility of Brönsted acid sites in zeolites, its validity as a criteria to quantify intrinsic acidity is more questionable. One of the reasons is that the ν(OH) vibration frequencies represent the ground state of the OH bond, which is related to homolytic dissociation and not to the heterolytic dissociation involved in protonation reactions. It was proposed by Kazansky et al. that the extinction coefficients of the ν(OH) stretching bands, which are proportional to the electric charges of protons, might be used as a measure of acidity. By combining DRIFT and ^{1}H NMR spectroscopies they showed that the extinction coefficients of acidic bridged hydroxyl groups in H-MOR, H-Y and H-ZSM-5 zeolites are several times higher than for the less acidic silanol groups, and the order of acidity found for the zeolites considered agrees with other estimations [42].

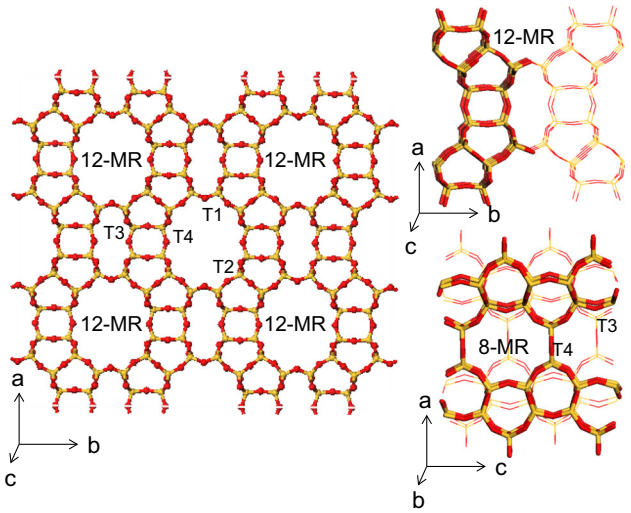

Fig. 2 Microporous structure of H-MOR zeolite

5 Measuring Acidity by Interaction of Brönsted Acid Sites with Base Molecules

By definition, Brönsted acidity is manifested when an acid interacts with a base and a proton is transferred:

$$AH + B \rightarrow AH{-}B \rightarrow A^- + BH^+.$$

Most methods for quantifying zeolite acidity are based on measuring the strength of the interaction of the Brönsted acid centers with probe molecules of increasing basicity. Weak bases are not protonated, but interact with the bridged hydroxyl groups through hydrogen bonding. Stronger bases become protonated by the acid sites, and in this case not only the intrinsic acidity of the Brönsted center, but also the proton affinity of the base molecule and the electrostatic interaction between the protonated conjugate base and the negatively charged zeolite framework play a role in the acid–base interaction.

A direct way to measure the strength of the acid–base interaction is adsorption calorimetry, which consists of dosing pulses of a reference base molecule onto a zeolite sample kept at a constant temperature into a microcalorimeter. The resulting heat flux pulse is integrated to obtain the corresponding heat of adsorption, so that for each pulse it is possible to determine the exact amount of base adsorbed and the energy released. Dosing continues until all acid sites are saturated, and in a typical microcalorimetry plot of adsorption enthalpy versus coverage, three types of sites of decreasing strength can usually be observed: Lewis acid sites with the lowest coverage, Brönsted acid sites, and reversible physisorption on the solid. It is a key point when using this technique to very carefully select the working temperature in order to minimize physisorption of the probe molecules, but still allowing sufficient mobility so that all available chemisorption sites are sampled [10, 14, 43–45].

Temperature programmed desorption (TPD) of ammonia (or other amines like pyridine, *n*-butyl amine, etc.) is one of the most widely used methods for characterizing acidity in zeolites. It is based on an initial saturation of the catalyst surface with chemisorbed ammonia molecules,

followed by a linear increase in the temperature in a flowing inert gas stream. Quantification of ammonia concentration can be done in the outlet gas at increasing temperature or, alternatively, the changes in the sample mass can be followed by carrying out the experiment in a microbalance. The amount of ammonia desorbing above a given characteristic temperature is taken as the concentration of acid sites, and adsorption enthalpies can be calculated from the peak desorption temperatures [9, 10, 14, 46, 47]. A common limitation of microcalorimetry and TPD techniques is that the Lewis or Brönsted nature of the adsorption sites is not distinguished, and no information about the structure of the acid centers is provided. To overcome this disadvantage, an improved method combining IR spectroscopy with ammonia TPD, named IRMS-TPD (infrared spectroscopy/mass spectrometry–temperature-programmed desorption), has been proposed [47–49]. The bending vibration band of NH_4^+ in zeolites at ca. 1450 cm^{-1} and the bands corresponding to bridged hydroxyl groups in the region between 3550 and 3650 cm^{-1} are followed at increasing temperatures, and simultaneously the concentration of desorbed ammonia is measured by mass spectrometry. With this method it was possible to calculate the desorption enthalpies of ammonia in 12-MR and 8-MR channels in zeolite H-MOR, 147 and 158 kJ mol^{-1}, respectively, and confirm the "higher acidity" (in fact, the higher desorption temperature or the higher stability of NH_4^+) of the Brönsted sites located in the smallest 8-MR pockets. Extension of this method to the study of other zeolite structures allowed to find a relationship between the ν(OH) vibration frequency of the Brönsted site and the ammonia desorption enthalpy determined by TPD, although the hydroxyl groups located in 6-MR strongly deviate from this relationship, probably due to the strong interactions existing between the acid proton and the neighboring framework O atoms located in such small rings.

IR spectroscopy of adsorbed base molecules is probably the most widely used technique to obtain information about Brönsted acid sites in zeolites [9, 10, 14, 50–52]. The interaction of a hydroxyl group with a weak base like CO or N_2 results in formation of a hydrogen bonded species that affects the vibrational modes of the OH bond. In particular, the ν(OH) stretching frequency shifts downward upon interaction with a base, and in principle it can be considered that a stronger acid site will undergo a larger shift in the ν(OH) stretching frequency. A logarithmic relationship between zeolite acid strength and Δν(OH) was reported by some authors [53]. In parallel, the CO stretching vibration ν(CO) shifts upward. When using infrared reflection absorption spectroscopy (IRAS), only modes with a component of the dynamic dipole moment normal to the surface can be observed due to the selection rules, which provides information about the adsorption geometry: if the ν(CO) frequency at 2180 cm^{-1} is observed, this means that the CO bond has a significant component perpendicular to the surface [54].

It is also possible to determine the standard enthalpy ΔH^0 and entropy ΔS^0 changes involved in the hydrogen bonding interaction between CO (or N_2) and zeolite Brönsted acid sites using the variable temperature infra red (VTIR) spectroscopy method [55, 56]. Using this methodology, a correlation between the enthalpy change ΔH^0 associated to hydrogen bonding and the shift in the OH vibration frequency Δν(OH) was reported for both CO and N_2 adsorption on HY, H-ZSM-5 and H-FER zeolites, but the trend did not apply to MWW type zeolites [57]. Calorimetric and ammonia TPD measurements, as well as calculated ΔH^0 values, indicate that H-MCM-22 has a weaker Brönsted acidity than H-ZSM5, but the Δν(OH) shifts due to adsorption of CO and N_2 are distinctively larger on H-MCM-22. This result highlights the difficulty to find a single indicator for quantifying Brönsted acidity in zeolites.

Stronger bases like ammonia or pyridine become protonated by the Brönsted acid sites, and new bands associated to the ammonium or pyridinium cations appear in the IR spectra. Pyridine has been widely used to characterize acid sites in zeolites because it allows to simultaneously determine the concentration of Brönsted and Lewis acid sites. Four vibrational modes at 1447–1460, 1488–1503, 1580, and 1600–1633 cm^{-1} are reported for pyridine coordinated to Lewis acid centers, while bands at 1485-1500, 1540 and 1640 cm^{-1} correspond to pyridinium cations. By measuring the relative intensity of those bands it is possible to estimate the number of Brönsted and Lewis acid sites able to retain pyridine at certain desorption temperatures [9, 54]. Moreover, the use of alkylpyridines with methyl, ethyl or *tert*-butyl substituents allows determining the accessibility of acid centers present in the microporous channels of zeolites [58].

6 Protonation and Formation of Reaction Intermediates

As previously mentioned, the protonation of a base by a zeolite acid site depends on the intrinsic acidity of the Brönsted center, but also on the proton affinity of the base molecule and the stabilizing interactions between the protonated conjugate base and the negatively charged zeolite framework. In this sense, it is important to remark that the reactant molecules in most zeolite-catalyzed processes of industrial interest are hydrocarbons (olefins or alkanes), which are considerably less basic than the amines or pyridines used as probe molecules to quantify acidity.

It was initially assumed that reaction mechanisms on acid zeolites are analogous to those in superacid media, and involve carbocationic intermediates formed by protonation of hydrocarbons by Brönsted acid sites [59, 60]. As shown in Scheme 1, trivalent carbenium ions could be formed by protonation of olefins or by protonation and dehydration of alcohols, while non-classical pentacoordinated carbonium ions can be formed by protonation of saturated alkanes [61, 62]. But solid state NMR and FTIR studies showed that simple carbenium ions are not stable within the zeolite microporous channels, and only some cyclic tertiary cations with a quite delocalized positive charge have been experimentally observed. Instead, surface alkoxide species with the alkyl group covalently bound to the zeolite framework have been reported as long-lived intermediates in the reactions of propene over acid zeolites or in the adsorption of 2-methyl-2-propanol on H-ZSM-5 [63–66], and have been identified as minima on the potential energy surfaces by means of quantum chemical calculations [67–76]. According to these theoretical studies, covalent alkoxides are formed by protonation of olefins π-bonded to Brönsted acid sites, following a concerted mechanism involving a cationic transition state in which the geometry and electronic structure of the organic fragment resembles that of a classical carbenium ion (Scheme 1b).

Both the calculated activation barriers for olefin protonation and the stability of the resulting covalent alkoxides depend on the olefin and on the type and size of the model used to simulate the zeolite catalyst. Thus, activation energies are mainly influenced by medium-range electrostatic effects, and reflect the order of stability of primary, secondary and tertiary carbenium ions. Alkoxide stability varies with olefin size, with bulkier alkoxides being less stable than smaller ones. Nevertheless, the result is more clearly marked by the local geometry of the active site and the degree of flexibility of the zeolite model. In particular, the *tert*-butoxide system formed by protonation of *iso*-butene is very sensitive to this factor, and it has been reported that the steric constraints due to the crystalline structure of a particular zeolite [73], and even to the particular position of the Al center in a given zeolite [74], are important enough to make the covalent *tert*-butoxide as unstable as the cationic *tert*-butyl carbenium ion. On the other hand, further stabilization of the organic fragment via hydrogen bonding with framework O atoms or by including dispersion interactions, allowed characterizing the *tert*-butyl carbenium ion as a reaction intermediate in the process of *iso*-butene protonation by zeolite Brönsted acid sites [74, 75]. An interesting conclusion from the study of olefin protonation at seven different positions in MOR zeolite [74] is that the best descriptor of alkoxide stability

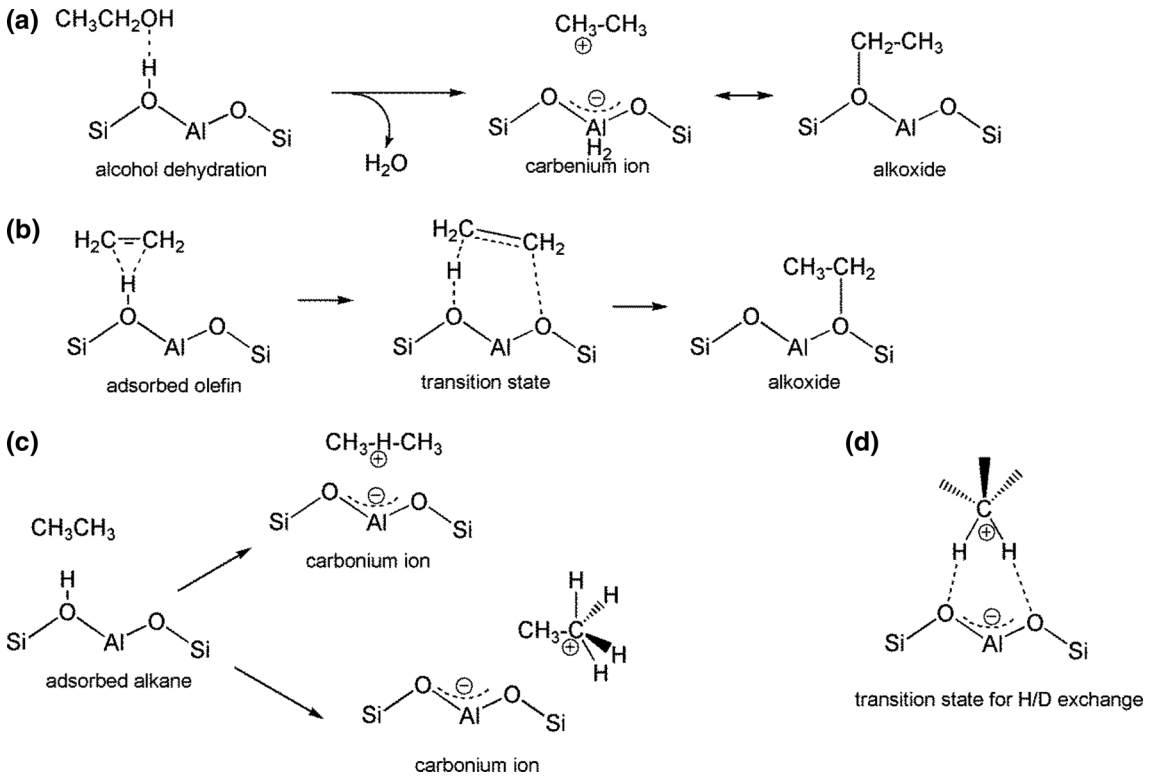

Scheme 1 Formation of carbenium ions or alkoxide intermediates by **a** alcohol dehydration and **b** olefin protonation at Brönsted acid sites. **c** Formation of carbonium ions by alkane protonation at Brönsted acid sites. **d** carbonium ion-like transition state for H/D exchange in alkanes

is the Al–O_b–Si angle, being O_b the framework oxygen atom involved in the O–C bond. The smaller the Al–O_b–Si angle, the more stable the alkoxide formed. Interestingly, the same relationship was previously observed for DPE [22], suggesting that the ability of the zeolite framework to accept the narrowing of the Al–O–Si angle associated to formation of a O–H or O–C bond is a key parameter governing its catalytic activity.

7 Reactivity of Alkoxide Intermediates

If quantifying acidity is not a simple task, relating acidity with reactivity is even more difficult. The reactivity of alkoxide groups formed at the Brönsted acid sites of zeolites has been experimentally investigated using in situ ^{13}C MAS NMR spectroscopy. Isotopically labelled ^{13}C-methoxide and ^{13}C-ethoxide groups formed by dehydration of $^{13}CH_3OH$ and $^{13}CH_3CH_2OH$, respectively, have been observed over acidic zeolites, and their subsequent alkylating activity when reacting with probe molecules like water, methanol, aromatics, ammonia, acetonitrile or carbon monoxide, as well as their participation in the methanol to olefin process, have been followed using this technique [13, 64, 77–81]. Under flow conditions, formation of surface methoxide species through methanol dehydration is greatly favored by the continuous removal of water, but in the presence of water methanol is readily regenerated. Hunger et al. reported that ^{13}C-methoxide groups react with methanol ($^{12}CH_3OH$) forming partially enriched $^{13}CH_3O^{12}CH_3$, which demonstrates the participation of the previously formed methoxide species as intermediates in the reaction of methanol conversion to dimethyl ether (DME) [79]. Using the same technique, surface methoxide species in H-Y, H-ZSM-5 and H-SAPO-34 catalysts were found to react with ammonia, HCl and aromatics like toluene to form methylamines, methyl chloride, and xylenes, respectively [13, 80, 81].

In the absence of other reactants, isolated methoxide groups on acidic zeolites are highly stable below 473 K, but at temperatures higher than 523 K the formation of hydrocarbons like propane, *iso*-butane and aromatics was observed on H-Y, H-ZSM-5 and H-SAPO-34 catalysts [13, 80]. The conversion of methanol to gasoline (MTG) or to light olefins (MTO) over acid zeolites are processes of great industrial interest [83, 84], but their mechanism is not yet fully understood despite the large research efforts devoted to this subject. It is generally accepted that methanol conversion to olefins is dominated by a "hydrocarbon pool" mechanism, according to which some organic impurities generate, during an initial induction period, a series of cyclic species like methylbenzenes and methylcyclopentenyl cations, which are the key intermediates that undergo repeated methylation and subsequent olefin elimination steps [64, 85–88]. However, the first C–C bond formation during the induction period is still a matter of debate [89], which is directly related to the activation of the C–H bond in surface methoxide species. On the basis of in situ ^{13}C MAS NMR data, Hunger et al. proposed that activation of the C–H bond of methoxide species in H-Y, H-ZSM-5 and H-SAPO-34 catalysts might be assisted by the adjacent basic oxygen atoms of the zeolite framework, resulting in formation of a carbene-like species that is more reactive towards alkane molecules and might explain the formation of the first C–C bond in the MTO process [13, 80]. Although Brönsted acidity is required to start this complex reaction, the catalytic performance of different zeolite materials in this process does not depend on the intrinsic acidity of their active centers, but many other factors like the ability to stabilize the species that form the "hydrocarbon pool" are more relevant.

8 Carbonium Ions as Reaction Intermediates

It has been proposed that the intermediate species in the zeolite-catalyzed monomolecular cracking and dehydrogenation of saturated alkanes are non-classical carbonium ions (see Scheme 1) and their formation and subsequent decomposition has been investigated by means of quantum chemical calculations [61, 62, 69, 90–92]. Using small H_3Si-OH-AlH_2-$OSiH_3$ or H_3Si–OH–$Al(OH)_2$–$OSiH_3$ cluster models to simulate a zeolite Brönsted acid site, Van Santen et al. proposed covalent alkoxides as reaction intermediates in many different zeolite-catalyzed hydrocarbon reactions, and concerted mechanisms involving ionic and ring-like transition states. Pentacoordinated carbonium ion-like transition states were described for H/D exchange in alkanes (Scheme 1d), while trivalent carbenium ion-type transition states were described for dehydrogenation and cracking of ethane [69, 91]. Using a similar cluster model, Corma et al. found that non-classical carbonium ions having a two-electron three-centre C–H–C bridge can be formed by direct protonation of a C–C bond in a linear alkane, while protonation of a C–H bond producing a carbonium ion with a pentacoordinated C atom is considerably less favored energetically (Scheme 1c) [61, 62, 92]. Important differences were found between homogeneous and heterogeneously catalyzed reaction mechanisms. In homogeneous media the mechanism of hydride transfer, alkylation, dehydrogenation and disproportionation reactions was explained in terms of different intramolecular rearrangements of a common carbonium ion intermediate. However, over a solid zeolite, only those carbonium ions in which the positive charge is delocalized and sterically inaccessible to framework oxygens exist as

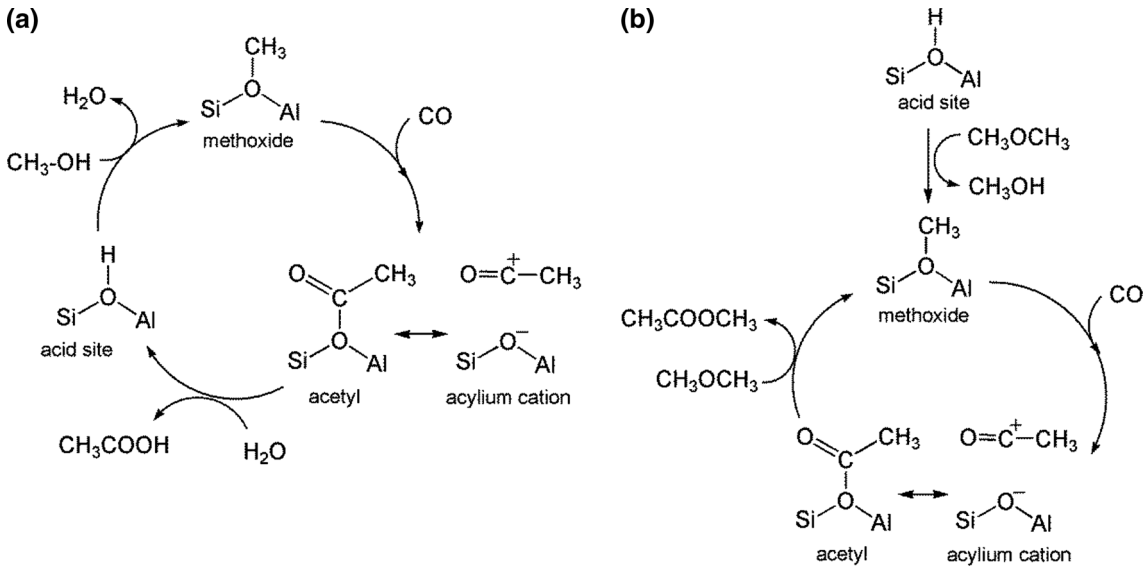

Scheme 2 Proposed mechanism for carbonylation of **a** methanol and **b** DME over acidic zeolites

reaction intermediates, that is, minima on the potential energy surface. Any transformation leading to charge localization results in a proton transfer to a framework oxygen, and therefore to formation of neutral molecules adsorbed on the Brönsted acid sites.

The role of the spatial constraints imposed by the zeolite microporous structure, that is not accounted for in the previously mentioned theoretical studies, has been carefully analyzed by Iglesia et al. [93–95]. The kinetics of monomolecular cracking and dehydrogenation of propane, *n*-butane and *iso*-butane within zeolites of different channel structure and at Brönsted sites located in channels of different size were investigated. It was found that the measured intrinsic activation barriers are quite similar on all zeolite samples, and are consistently higher for dehydrogenation than for cracking. However, turnover rates for both reactions were found considerably higher on Brönsted acid sites located within the smaller 8-MR pockets of H-MOR zeolite. The channel environment around a Brönsted acid site strongly influences the stabilization of the cationic transition state. Reactants and transition states are only partially confined in the 8-MR side pockets of mordenite, which results in important entropy gains that compensate the losses in enthalpy and lead to a lower free energy activation barrier. Such entropy effects dominate the kinetics of reactions occurring at high temperature, like alkane activation, while are less important for reactions occurring at lower temperatures [93–95]. The important conclusion of these studies is that the intrinsic acidity of the Brönsted acid site at which the process occurs does not determine the reaction rate, but other factors associated to local interactions between the reactant, transition state or reaction intermediate and the zeolite walls around the active site, are more relevant.

9 Selectivity and Site Specificity in Zeolites

A nice example of site specificity in zeolites is the selective carbonylation of methanol with CO catalyzed by mordenite. Acetic acid is formed by reaction of methanol (or dimethyl ether DME) with CO on different zeolites like HY, H-ZSM-5, H- FER and H-MOR, being the two last materials the most active and selective [82, 96, 97]. The proposed reaction mechanism starts with formation of a surface methoxide group by dehydration of methanol on a Brönsted acid site. The rate determining step is the reaction of the methoxide group with CO to form an acylium cation or an acetyl intermediate, which reacts with water yielding acetic acid and regenerating the Brönsted acid site (Scheme 2a). When DME is used instead of methanol, its reaction with the acetyl intermediate produces methyl acetate and regenerates the surface methoxide group (Scheme 2b) [5, 82, 97].

This mechanism was verified by ^{13}C MAS NMR spectroscopy [13, 81, 98], and no acylium cations but covalent acetyl species were identified as the reaction intermediates [82, 98]. Since the common feature of H-FER and H-MOR is the presence of 8-MR, it was proposed that the reaction of methoxide groups with CO occurs selectively within these channels, while Brönsted sites present in larger 10-MR or 12-MR channels catalyze the formation of hydrocarbons that leads to catalyst deactivation [39]. To identify the active and selective sites for methanol

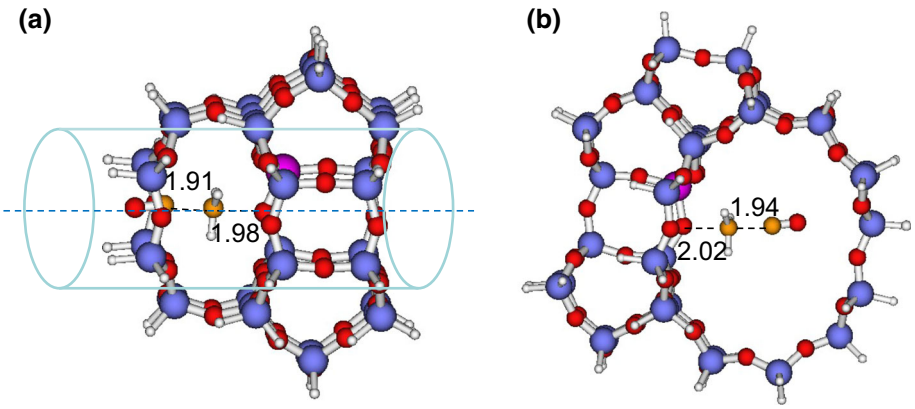

Fig. 3 Optimized geometry of the transition states for the reaction of CO with methoxide groups at **a** T3-O33 (inside 8-MR pocket) and **b** T4-O44 (main 12-MR channel) positions in H-MOR, and schematic representation of the relative orientation of the O–CH_3–CO bond and the channel axis at T3-O33

carbonylation and understand the role of pore size and local geometry of the active site, the mechanism of methanol carbonylation at different positions in H-MOR was investigated by means of DFT calculations [99, 100]. It was found that the reaction of methoxy groups with CO does not occur at all sites located within 8-MR channels, but only when the methoxy group is formed at the T3-O33 position inside the side pockets of mordenite the process is selective towards carbonylation. The reason is the unusual orientation of the methoxy group in relation to the 8MR channel (Fig. 3), that allows a perfect fitting between the transition state for CO attack and the framework oxygen atoms, while the attack of bulkier nucleophiles like methanol (leading to DME formation) or DME is sterically forbidden. On the other hand, van der Waals interactions are more important in the narrow 8MR channels than in the larger 12MR channels, leading to a larger stabilization of the transition states and a decrease in the activation barriers when the process takes place inside the 8MR pockets. Altogether, the particular orientation of the intermediate methoxy species parallel to the 8MR channel axis is the origin of the unique selectivity towards carbonylation obtained when using H-MOR as catalyst [95, 99, 100].

10 Summary

Acid zeolites are widely used as heterogeneous catalysts for hydrocarbon reactions of industrial interest, due to their high activity, selectivity, and thermal stability. Brönsted acidity is associated to bridged hydroxyl groups Al–O(H)–Si, and attempts have been done to quantify the number and strength of the zeolite acid sites and to correlate this acidity with the catalytic activity towards different reactions. Research over the last 25 years has demonstrated that the excellent catalytic performance of zeolites is not only due to a strong acidity, but other factors associated to their microporous structure of channels and cavities are even more relevant. Thus, selectivity effects related to diffusion of reactants and products through the internal channels, stabilization of charged species by electrostatic interactions with the zeolite framework, steric constraints on reaction intermediates and transition states, and site specificity for particular reactions are key to understand the catalytic performance of acid zeolites.

Acknowledgments The authors thank the Spanish Science and Innovation Ministry (Consolider Ingenio 2010-MULTICAT CSD2009-00050 Project and Subprograma de apoyo a Centros y Universidades de Excelencia Severo Ochoa SEV 2012 0267) and Generalitat Valenciana (PROMETEOII/2013/011 Project) for financial support.

References

1. Corma A (1997) Chem Rev 97:2373–2419
2. Clerici MG (2000) Top Catal 13:373–386
3. Corma A (2003) J Catal 216:298–312
4. Haw F, Song W, Marcus DM, Nicholas JB (2003) Acc Chem Res 36:317–326
5. Bahn A, Iglesia E (2008) Acc Chem Res 41:559–567
6. Yilmaz B, Müller U (2009) Top Catal 52:888–895
7. Martínez C, Corma A (2011) Coord Chem Rev 255:1558–1580
8. Cejka J, Centi G, Pérez-Pariente J, Roth WJ (2012) Catal Today 179:2–15
9. Corma A (1995) Chem Rev 95:559–614
10. Farneth WE, Gorte RJ (1995) Chem Rev 95:615–635
11. Van Santen RA, Kramer GJ (1995) Chem Rev 95:637–660
12. Cejka J, van Bekkum H, Corma A, Schüth F (2007) Introduction to Zeolite Molecular Sieves, 3rd edn. Elsevier, Amsterdam, pp 1–1094
13. Wang W, Hunger M (2008) Acc Chem Res 41:895–904
14. Derouane EG, Védrine JC, Ramos Pinto R, Borges PM, Costa L, Lemos MANDA, Lemos F, Ramôa Ribeiro F (2013) Catal Rev 55:454–515
15. Sauer J (1989) Chem Rev 89:199–255
16. Brönsted J (1928) Chem Rev 5:231–338
17. Strodel P, Neyman KM, Knözinger H, Rösch N (1995) Chem Phys Lett 240:547–552
18. Chatterjee A, Iwasaki T, Ebina T, Miyamoto A (1998) Microp Mesop Mater 21:421–428
19. Yuan SP, Wang JG, Li YW, Jiao H (2002) J Phys Chem A 106:8167–8172
20. Brand HV, Curtiss LA, Iton LE (1993) J Phys Chem 97:12773–12782
21. Brand HV, Curtiss LA, Iton LE (1992) J Phys Chem 96:7725–7732

22. Kassab E, Seiti K, Allavena M (1998) J Phys Chem 92:6705–6709
23. Jones AJ, Carr RT, Zones SI, Iglesia E (2014) J Catal 3121:58–68
24. Jungsuttiwong S, Lomratsiri J, Limtrakul J (2011) Int J Q Chem 111:2275–2282
25. Sauer J, Schröder J, Temath K-PV (1998) Coll Czech Chem Commun 63:1394–1408
26. Sauer J, Sierka M (2000) J Comput Chem 21:1470–1493
27. Haase F, Sauer J (2000) Micr Mesop Mater 35–36:379–385
28. Eichler U, Brändle M, Sauer J (1997) J Phys Chem B 101:10035–10050
29. Brändle M, Sauer J (1998) J Am Chem Soc 120:1556–1570
30. Lercher JA, Jentys A (2007) Infrared and Raman spectroscopy for characterizing zeolites. In: van Bekkum H, Cejka J, Corma A, Schüth F (eds) Introduction to zeolite science and practice, 3rd edn. Elsevier, Amsterdam
31. Klinowski J (1991) Chem Rev 91:1459–1479
32. Knözinger H, Huber SJ (1998) Chem Soc Faraday Trans 94:2047–2059
33. Jacobs PA, von Ballmoos R (1982) J Phys Chem 86: 3050–3052
34. Biaglow AI, Parrillo DJ, Gorte RJ (1993) J Catal 144:193–201
35. Aufdembrink BA, Dee DP, McDaniel PL, Mebrahtu T, Slager TL (2003) J Phys Chem B 107:10025–10031
36. van Well VJM, Cottin X, de Haan JW, Smit B, Nivarthy G, Lercher JA, van Hooff JHC, van Santen RA (1998) J Phys Chem B 102:3945–3951
37. van Well VJM, Cottin X, Smit B, van Hooff JHC, van Santen RA (1998) J Phys Chem B 102:3952–3958
38. Marie O, Massiani P, Thibault-Starzyk F (2004) J Phys Chem B 108:5073–5081
39. Bhan A, Allian AD, Sunley GJ, Law DJ, Iglesia E (2007) J Am Chem Soc 129:4919–4924
40. Bevilacqua M, Busca G (2002) Catal Commun 3:497–502
41. Jacobs PA, Mortier JW (1982) Zeolites 2:226–230
42. Kazansky VB, Serykh AI, Semmer-Herledan V, Fraissard J (2003) Phys Chem Chem Phys 5:966–969
43. Cardona-Martinez N, Dumesic JA (1990) J Catal 125:427–444
44. Auroux A (2002) Top Catal 19:205–213
45. Auroux A (2008) Mol Sieves 6:45–152
46. Rodríguez-González L, Hermes F, Bertmer M, Rodríguez-Castellón E, Jiménez-López A, Simon U (2007) Appl Catal A Gen 328:174–182
47. Niwa M, Katada N (2013) Chem Rec 13:432–455
48. Niwa M, Nishikawa S, Katada N (2005) Microporous Mesoporous Mater 82:105–112
49. Suzuki K, Noda T, Katada N, Niwa M (2007) J Catal 250:151–160
50. Zecchina A, Otero Arean C (1996) Chem Soc Rev 25:187–197
51. Knözinger H (1997) In: Ertl G, Knözinger H, Weitkamp J (eds) Handbook of Heterogeneous Catalysis, vol 2. VCH, Weinheim, p 707
52. Hadjiivanov K, Vayssilov G (2002) Adv Catal 47:307–511
53. Frash MV, Makarova MA, Rigby AM (1997) J Phys Chem B 101:2116–2119
54. Boscoboinik JA, Yu X, Emmez E, Yang B, Shaikhutdinov S, Fischer FD, Sauer J, Freund HJ (2013) J Phys Chem C 117:13547–13556
55. Garrone E, Otero Arean C (2005) Chem Soc Rev 34:846–857
56. Nachtigall P, Delgado MR, Nachtigallova D, Otero Arean C (2012) Phys Chem Chem Phys 14:1552–1569
57. Otero Arean C, Delgado MR, Nachtigall P, Thang HV, Rubes M, Bulanek R, Chlubna-Eliasova P (2014) Phys Chem Chem Phys 16:10129–10141
58. Nesterenko NS, Thibault-Starzyk F, Montouillout V, Yushchenko VV, Fernandez C, Gilson JP, Fajula F, Ivanova I (2006) Kinet Catal 47:40–48
59. Jacobs PA (1977) Carbonigenic activity of zeolites. Elsevier, New York
60. Tanabe K, Misono M, Ono Y, Hattori H (1989) New solid acids and bases. Elsevier, New York
61. Corma A, Planelles J, Sánchez-Marin J, Tomás F (1985) J Catal 93:30–37
62. Boronat M, Corma A (2008) Appl Catal A 336:2–10
63. Haw JF, Nicholas JB, Xu T, Beck LW, Ferguson DB (1996) Acc Chem Res 29:259–267
64. Haw JF (2002) Phys Chem Chem Phys 4:5431–5441
65. Yang S, Kondo JN, Domen K (2002) Catal Today 73:113–125
66. Aronson MT, Gorte RJ, Farneth WE, White D (1989) J Am Chem Soc 111:840–846
67. Kazansky VB (1991) Acc Chem Res 24:379–383
68. Kazansky VB, Frash MV, Van Santen RA (1996) Appl Catal A 146:225–247
69. Rigby AM, Kramer GJ, Van Santen RAJ (1997) Catal A 170:1–10
70. Sinclair PE, de Vries A, Sherwood P, Catlow CRA, Van Santen RAJ (1998) Chem Soc Faraday Trans 94:3401–3408
71. Boronat M, Zicovich-Wilson CM, Viruela PM, Corma A (2001) J Phys Chem B 105:11169–11177
72. Rozanska X, Demuth Th, Hutschka F, Hafner J, Van Santen RA (2002) J Phys Chem B 106:3248–3254
73. Rozanska X, Van Santen RA, Demuth Th, Hutschka F, Hafner J (2003) J Phys Chem B 107:1309–1315
74. Boronat M, Viruela PM, Corma A (2004) J Am Chem Soc 126:3300–3309
75. Tuma C, Sauer J (2005) Angew Chem Int Ed 44:4769–4771
76. Nieminen V, Sierka M, Murzin DY, Sauer J (2005) J Catal 231:393–404
77. Ivanova II, Corma A (1997) J Phys Chem B 101:547–551
78. Wang W, Seiler M, Ivanova I, Weitkamp J, Hunger M. Chem Commun 2001, 1362–1363
79. Wang W, Seiler M, Hunger M (2001) J Phys Chem B 105:12553–12558
80. Wang W, Buchholz A, Seiler M, Hunger M (2003) J Am Chem Soc 125:15260–15267
81. Jiang Y, Hunger M, Wang W (2006) J Am Chem Soc 128:11679–11692
82. Cheung P, Bhan A, Sunley GJ, Law DJ, Iglesia E (2007) J Catal 245:110–123
83. Stöcker M (1999) Microporous Mesoporous Mater 29:3–48
84. Keil FJ (1999) Microporous Mesoporous Mater 29:49–66
85. Dahl IM, Kolboe S (1994) J Catal 149:458–464
86. Dahl IM, Kolboe S (1996) J Catal 161:304–309
87. Haw JF, Nicholas JB, Song W, Deng F, Wang Z, Xu T, Heneghan CS (2000) J Am Chem Soc 122:4763–4775
88. Arstad B, Nicholas JB, Haw F (2004) J Am Chem Soc 126:2991–3001
89. Lesthaeghe D, Van Speybroeck V, Marin GB, Waroquier M (2006) Angew Chem Int Ed 45:1714–1719
90. Collins SJ, O'Malley PJ (1995) J Catal 153:94–99
91. Blaszkowski SR, Nascimento MAC, van Santen RA (1996) J Phys Chem 100:3463–3472
92. Boronat M, Viruela PM, Corma A (2000) Phys Chem Chem Phys 2:3327–3333
93. Gounder R, Iglesia E (2009) J Am Chem Soc 131:1958–1971
94. Gounder R, Jones AJ, Carr RT, Iglesia E (2012) J Catal 286:214–223
95. Gounder R, Iglesia E (2012) Acc Chem Res 45:229–238
96. Fujimoto K, Shikada T, Omata K, Tominaga H (1984) Chem Lett 12:2047–2050

97. Cheung P, Bhan A, Sunley GJ, Iglesia E (2006) Angew Chem Int Ed 45:1617–1620
98. Lezcano-González I, Vidal-Moya JA, Boronat M, Blasco T, Corma A (2013) Angew Chem Int Ed 52:5138–5141
99. Boronat M, Martínez C, Law D, Corma A (2008) J Am Chem Soc 130:16316–16323
100. Boronat M, Martínez C, Corma A (2011) Phys Chem Chem Phys 13:2603–2612